Raman scattering from phonons and magnons in $RFe_3(BO_3)_4$

Daniele Fausti,* Agung A. Nugroho, and Paul H.M. van Loosdrecht†
Material Science Centre, University of Groningen, 9747 AG Groningen, The Netherlands

Sergei A. Klimin and Marina N. Popova
Institute of Spectroscopy, RAS, 142190, Troitsk, Moscow Region, Russia

Leonard N. Bezmaternykh
L.V. Kirensky Institute of Physics, Siberian Branch of RAS, Krasnoyarsk, 660036, Russia
(Received 19 December 2005; revised manuscript received 27 April 2006; published 7 July 2006)

Inelastic light scattering spectra of several members of the $RFe_3(BO_3)_4$ family reveal a cascade of phase transitions as a function of temperature, starting with a structural, weakly first-order, phase transition followed by two magnetic phase transitions. Those consist of the ordering of the Fe-spin sublattice, revealed by all the compounds, and a subsequent spin-reorientational transition for $GdFe_3(BO_3)_4$. The Raman data evidence a strong coupling between the lattice and magnetic degrees of freedom in these borates. The Fe-sublattice ordering leads to a strong suppression of the low-energy magnetic scattering, and a multiple peaked two-magnon scattering continuum is observed. Evidence for short-range correlations is found in the "paramagnetic" phase by the observation of a broad magnetic continuum in the Raman data, which persists up to surprisingly high temperatures.

DOI: 10.1103/PhysRevB.74.024403 PACS number(s): 75.40.Gb, 63.22.+m, 75.30.−m, 64.70.Kb

I. INTRODUCTION

The family of $RM_3(BO_3)_4$ crystals (R=Y or a rare earth, M=Al, Ga, Sc, Cr, Fe) has attracted considerable attention during the last several years. Different combinations of R and M lead to a large variety of physical properties that, together with their excellent physical characteristics and chemical stability, make these crystals extremely interesting both from application and fundamental points of view. The lack of inversion symmetry (they crystallize in a trigonal space group) has stimulated different applications in the field of optical and optoelectronic devices. Crystals of $YAl_3(BO_3)_4$ and $GdAl_3(BO_3)_4$ doped with Nd have been widely studied and used in optical devices, for self-frequency doubling and self-frequency summing lasers.[1–3] Concentrated $NdAl_3(BO_3)_4$ crystals are efficient media for mini-lasers.[3] Rare-earth borates with magnetic ions (M=Cr, Fe) are much less studied. Recently, some iron borates were reported to possess multiferroic features, demonstrating the coexistence of magnetic and ferroelectric order parameters,[4] they may therefore be considered for optoelectronic applications. These magnetic borates are also expected to exhibit interesting magnetic properties because of the presence of two different kinds of magnetic ions (3*d* and 4*f* elements) and, in particular, because their structure features isolated helicoidal chains of magnetic 3*d* atoms.

The crystal structure of $RM_3(BO_3)_4$ borates belongs to the structural type of the natural mineral huntite $CaMg_3(CO_3)_4$ that crystallizes in the space group *R*32 of the trigonal system.[5–8] The primitive unit cell contains one formula unit. Three kinds of coordination polyhedra are present, trigonal prisms for RO_6, octahedra for MO_6, and two types of planar triangular BO_3 groups: equilateral $B1O_3$ and isosceles $B2O_3$ (the numbering of inequivalent ions position is the same as in Ref. 8). The MO_6 octahedra share edges forming mutually independent helicoidal chains that run parallel to the *c* axis (see Fig. 1). The RO_6 prisms are isolated polyhedra, each of them connects three helicoidal MO_6 chains, while there are no direct R-O-R links between different RO_6 prisms. This structure can also be seen as a succession of alternating BO_3 and R+M layers perpendicular to the *c* axis.

Recently, a systematic study of rare-earth iron borates $RFe_3(BO_3)_4$ (R=Y, La-Nd, Sm-Ho) was undertaken for polycrystalline samples.[9] The measurements of magnetization, specific heat, and ^{57}Fe Mössbauer spectra revealed an antiferromagnetic ordering at low temperatures. The magnetic ordering temperature increases with decreasing R^{3+} ionic radius, from 22 K for $LaFe_3(BO_3)_4$ to 40 K for $TbFe_3(BO_3)_4$. In addition to this, x-ray diffraction, specific heat measurements, and differential thermal analysis have

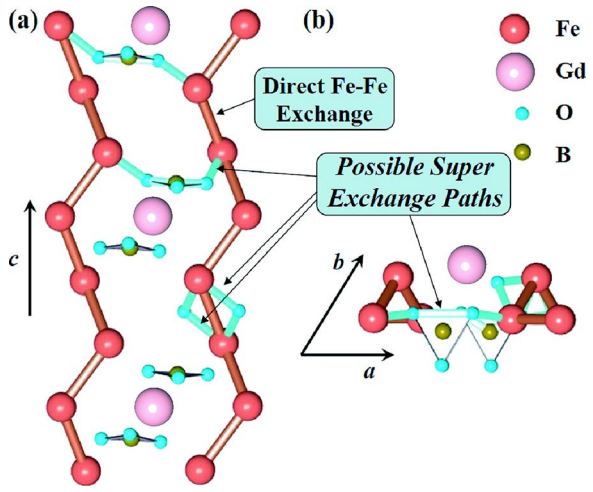

FIG. 1. (Color online) The structure of $RM_3(BO_3)_4$ incorporates helicoidal chains of M^{3+} ions. The figure shows the structure of iron borates (M=Fe) viewed from different angles: (a) perpendicular to the C_3 axis and (b) parallel to it. The possible exchange paths are also shown.

indicated a structural phase transition for $RFe_3(BO_3)_4$ compounds with R=Eu-Ho, Y. Its temperature increases with decreasing R^{3+} ionic radius, from 88 K for $EuFe_3(BO_3)_4$ to 445 K for $YFe_3(BO_3)_4$. Magnetic ordering of the La- and Nd-iron borates has been confirmed by spectroscopic and magnetic measurements on nonoriented single crystals.[7,10] Studies on oriented single crystals have only been carried out for $GdFe_3(BO_3)_4$, using a variety of methods.[4,8,11–14] Recent specific heat, Raman scattering, and Nd^{3+} probe absorption measurements revealed a cascade of three spontaneous phase transitions in $GdFe_3(BO_3)_4$.[12] A structural, weakly first-order, phase transition into a less symmetric low-temperature phase was found at T_S=156 K [this in contrast to the powder result T_S=174 K (Ref. 9)]. At lower temperature, two magnetic transitions have been observed. A second-order phase transition occurs at 37 K, resulting in an antiferromagnetic ordering of the Fe spin sublattice. This transition is accompanied by a polarization of the Gd spin subsystem. The second magnetic transition is observed at 9 K and has been identified as a first-order Fe spin-reorientation transition.[12] A detailed picture of magnetic phase transitions in $GdFe_3(BO_3)_4$ as a function of temperature and magnetic field has recently been suggested in Ref. 13 on the basis of antiferromagnetic resonance studies.

Quite recently, the low-temperature structural phase of $GdFe_3(BO_3)_4$ has been identified as a $P3_121$ trigonal structure.[8] We have found no information on the low-temperature structure of other rare-earth iron borates. Such information can be obtained from the comparison of low-temperature Raman spectra of $GdFe_3(BO_3)_4$ and other compounds from the $RFe_3(BO_3)_4$ family. Raman studies of $RFe_3(BO_3)_4$ were performed for R=La and Nd at room temperature.[15] Preliminary temperature-dependent results on the R=Gd compound have also been reported recently.[12]

The present work investigates two different aspects of the rare-earth iron borates. First, inelastic light scattering studies of the vibrational and structural properties of different $RFe_3(BO_3)_4$ are presented. Among others they reveal the weak first-order phase transition from the high-temperature $R32$ structure to the low-temperature $P3_121$ one. The second part of this paper focuses on the magnetic properties. Apart from observing changes in phonon frequencies at the antiferromagnetic ordering transition arising from magnetoelastic couplings, the spectra also exhibit relatively strong two-magnon scattering features. The magnetically ordered phases exhibit well-defined magnon excitations, resulting in a multiple peaked scattering continuum at finite energy. In the paramagnetic phase, a strong low-energy continuum is found, which results from the persistence of short-range correlations in the helicoidal Fe spin chains up to quite high temperatures.

II. EXPERIMENTAL DETAILS

Different samples of $RFe_3(BO_3)_4$, with R = Gd, Nd, Tb, Er, and Y were grown using a $Bi_2Mo_3O_{12}$-based flux, as described in Refs. 16 and 17. Unlike the Bi_2O_3-based fluxes,[7] in $Bi_2Mo_3O_{12}$-based flux Bi_2O_3 is strongly bonded to MoO_3, which excludes a partial substitution of bismuth for a rare earth during crystallization. Spontaneous nucleation from the flux resulted in small single crystals ($1\times1\times1$ mm). We used these crystals as seeds to grow large ($10\times5\times5$ mm) single crystals of Gd, Nd, and Tb iron borates. As for $ErFe_3(BO_3)_4$ and $YFe_3(BO_3)_4$, only small single crystals of these compounds were studied in this work. All the crystals were green in color. The samples were oriented either by x-ray-diffraction technique or by using their morphology and optical polarization methods.

The Raman measurements were performed in a backscattering configuration, using a three-grating micro-Raman spectrometer (T64000 Jobin Yvon) equipped with a liquid nitrogen-cooled charged coupled device (CCD) detector. The frequency resolution was better that 1 cm^{-1} for the frequency region considered. The samples were placed in a optical microscope cryostat. The temperature was varied from 2.7 to 500 K, with a stability of ±0.02 K with the aid of RhFe resistor which was placed near the sample. The scattering was excited by the second harmonic light of a $Nd:YVO_4$ laser (532 nm), focused down to ~50 μm^2 with the power density on the sample kept below 0.1 $mW/\mu m^2$. The polarization was controlled both on the incoming and outgoing beams, giving access to all relevant polarization combinations.

Most of the experiments were performed with light incident perpendicular to the C_3-axis of the crystal, $\vec{k}\perp c$ [as a rule, precise orientation of $\vec{k}$ in the (ab) plane was not known], however, when the shape of the samples allowed, also the $\vec{k}||c$ configuration has been employed. Spectra are marked using the Porto notation.[18] For $\vec{k}\perp c$, only the polarization of incident and scattered light are indicated. The conventions $z||C_3$, $x||C_2$ are used to describe the geometry of the Raman experiments. We were able to obtain only partially polarized Raman spectra of $ErFe_3(BO_3)_4$ and $YFe_3(BO_3)_4$.

Preliminary dielectric measurements were performed for $RFe_3(BO_3)_4$ on nonoriented crystals of typical size $1\times1\times0.2$ mm^3. The surfaces were polished and covered with Ag paste, and the electrical contacts were made using Pt wires connected to the surface by additional Ag paste. The samples were mounted on a homemade insert for a Quantum Design PPMS system. The capacitance was measured using a Andeen-Hagerling AH2500A capacitance bridge operating at a fixed frequency of 1 kHz.

III. EXPERIMENTAL RESULTS

The room-temperature (RT) spectra of $GdFe_3(BO_3)_4$ for all studied experimental configurations are presented in Fig. 2. The regions where the internal BO_3 vibrations are expected are indicated by the horizontal bars in the top of the panel. The spectra show a strong dependence on the polarization of the incoming and scattered light, but also show a distinct difference between ($xx+yy+xy$) polarized spectra for $\vec{k}$ parallel to c and for $\vec{k}$ perpendicular to c. The spectra for different rare-earth iron borates are, as expected, qualitatively quite similar, as is shown in Fig. 3.

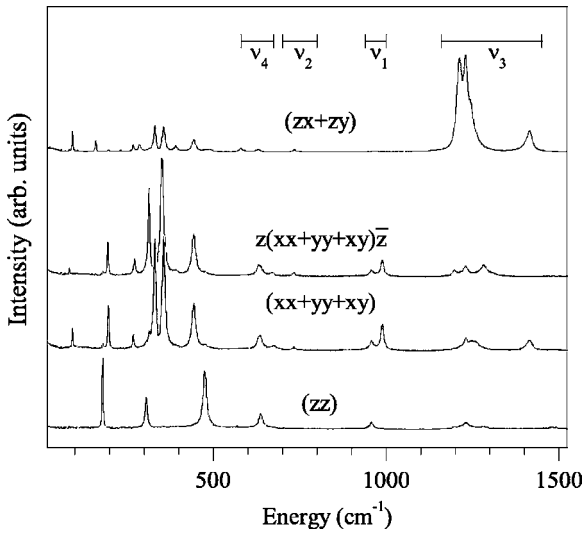

FIG. 2. Polarized Raman spectra of $GdFe_3(BO_3)_4$ at room temperature. The bars at the top indicate the frequency regions for the internal vibrations of BO_3 groups.

The phonon lines narrow progressively with lowering the temperature and several new modes appear abruptly in $GdFe_3(BO_3)_4$, $TbFe_3(BO_3)_4$, $ErFe_3(BO_3)_4$, and $YFe_3(BO_3)_4$, at T_S=155, 198, 340, and 350 K, respectively. Figures 4 and 5 and Table I give a detailed comparative picture of the phonon modes observed above and below T_S in $RFe_3(BO_3)_4$. The intensities of the new modes show a hysteresis as a function of temperature (see Fig. 6). The lowest-frequency intense new mode appears abruptly below the phase transition, but then exhibits a soft-mode-like behavior with further lowering of the temperature; i.e., for $GdFe_3(BO_3)_4$ and $TbFe_3(BO_3)_4$ the low-frequency mode shifts from 26 cm^{-1} at T_S to, respectively, 56 cm^{-1} and 57 cm^{-1} at 3 K, and for $ErFe_3(BO_3)_4$ and $YFe_3(BO_3)_4$, it goes respectively from 25 to 72 cm^{-1} and from 27 to 76 cm^{-1}. At the same time, its linewidth decreases from 12 to 3 cm^{-1} [see Figs. 7 and 4(b)]. The spectra in $(xz+yz)$ polarization of all the compounds demonstrate a low-frequency scattering continuum that gradually changes its shape with lowering the temperature and exhibits the opening of a "gap" at T_N (see Fig. 8). For $NdFe_3(BO_3)_4$ at the lowest temperatures, a well-defined narrow peak at about 10 cm^{-1} is observed within the gap. This mode shifts to zero frequency and strongly broadens upon approaching T_N from below [Fig. 8(d)]. For the Gd compound, a similar mode is observed below T_N at about 18 cm^{-1} [Fig. 8(e)].

IV. GROUP-THEORETICAL ANALYSIS

A. High-temperature structure $R32$ (D_3^7)

The primitive cell of the high-temperature structure $R32$ of $RFe_3(BO_3)_4$ contains 20 atoms, which results in 57 vibrational normal modes. Knowing the local symmetry of all the atomic positions, one can perform the factor-group analysis to find the symmetries of these modes.[18,19] R and B1 atoms reside in highly symmetric D_3 positions.[7,8] and generate A_2

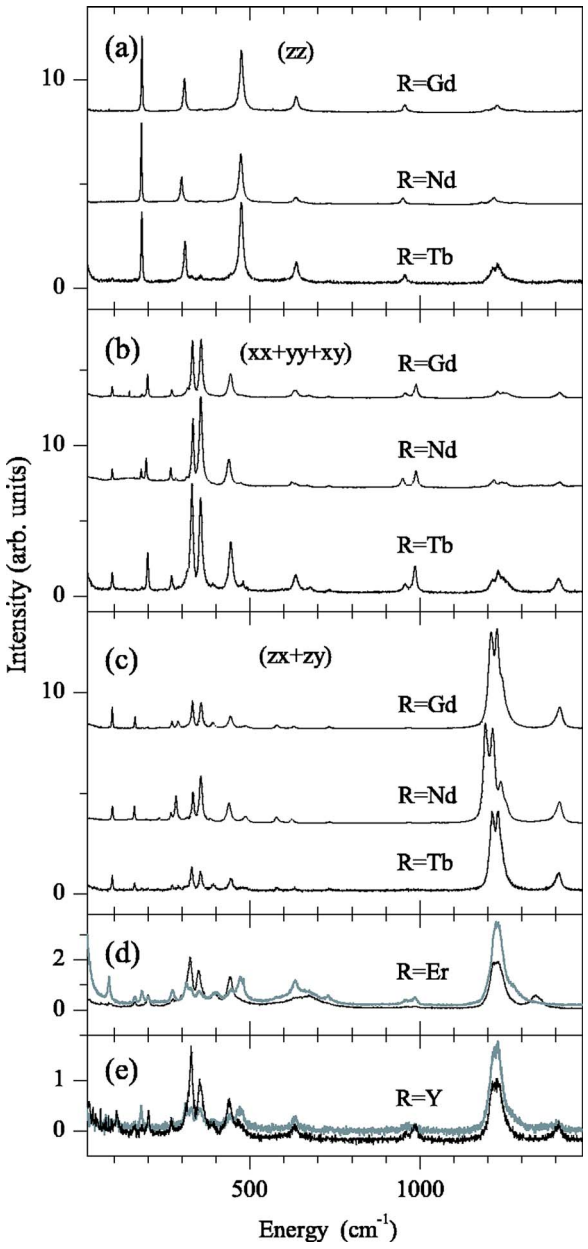

FIG. 3. (Color online) (a–c) Polarized Raman spectra for $RFe_3(BO_3)_4$, R=Gd, Nd, Tb, at room temperature. (d,e) Partially polarized Raman spectra for (d) $ErFe_3(BO_3)_4$ at 390 K and (e) $YFe_3(BO_3)_4$ at 420 K.

$\oplus E$ modes each. Fe, B2, O1, and O2 atoms are in C_2 symmetry positions, which results in $A_1 \oplus 2A_2 \oplus 3E$ modes for each of them. O3 atoms occupy general C_1 positions and give $3A_1 \oplus 3A_2 \oplus 6E$ modes. Summing all these modes and subtracting the $A_2 \oplus E$ acoustic modes, one gets the following optical vibrational modes of the crystal, in accordance with the results of Ref. 15:

$$\Gamma_{\text{vibr}} = 7A_1(xx,yy,zz) \oplus 12A_2(E//z) \oplus 19E(E//x,E//y,xz,yz,xy). \quad (1)$$

Notations in parentheses refer to the allowed components of electric dipole moment [infrared (IR) activity] and the

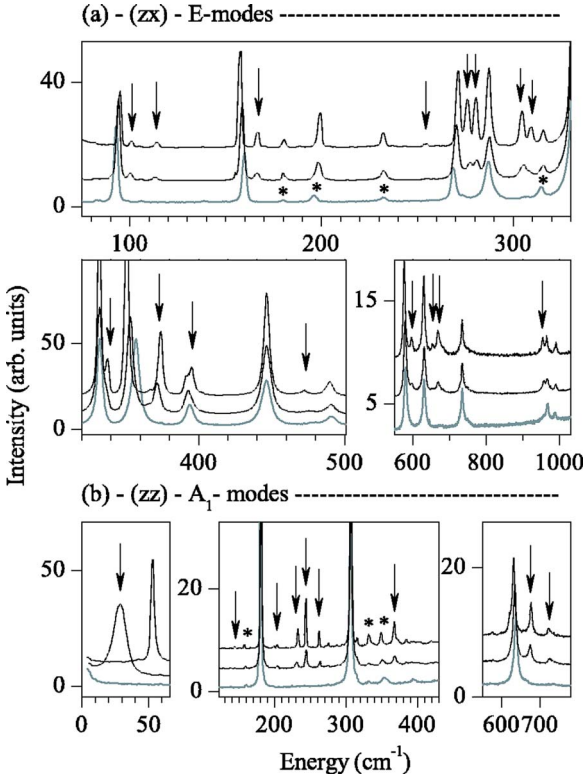

FIG. 4. (Color online) Raman spectra of $GdFe_3(BO_3)_4$ above and below T_s=156 K, namely, at 161 K (the lowest traces in each panel), 150 K (middle traces), and 30 K (upper traces). (a) ($zx+zy$) polarization. (b) (zz) polarization. New modes that appear below T_s are indicated by arrows. Asterisks mark the lines from another polarization.

polarizability tensor (Raman activity). Doubly degenerated E modes are polar and both IR and Raman active. The light propagating along the c axis ($\vec{k}||c$) probes TO modes, while the $\vec{k} \perp c$ configuration gives pure LO modes.[15]

The strongest bonds in the structure of $RFe_3(BO_3)_4$ borates are B-O bonds within the planar BO_3 triangles. Considering them as molecular units that occupy D_3 (for $B1O_3$) and C_2 (for $B2O_3$) positions, and adding the modes of translational character coming from R and Fe ions (respectively, in D_3 and C_2 position), we obtain the following optical modes:

$$\Gamma_{\text{vib}}^{tr} = 2A_1 \oplus 5A_2 \oplus 7E; \quad \Gamma_{\text{vib}}^{\text{lib}} = A_1 \oplus 3A_2 \oplus 4E, \qquad (2)$$

where the librational ones (right equation) come from the BO_3 units. The total number of external optical vibrations is, thus,

$$\Gamma_{\text{vib}}^{\text{ext}} = 3A_1 \oplus 8A_2 \oplus 11E. \qquad (3)$$

Subtracting (2) from (1), one gets the internal vibrational modes related to the vibrations of BO_3 groups

$$\Gamma_{\text{vib}}^{\text{int}} = 4A_1 \oplus 4A_2 \oplus 8E. \qquad (4)$$

The correlation scheme of Fig. 9 helps to get a deeper insight into the origin of the vibrational modes of $RFe_3(BO_3)_4$. It follows from this scheme that two of the seven A_1 modes originate from the fully symmetric vibration

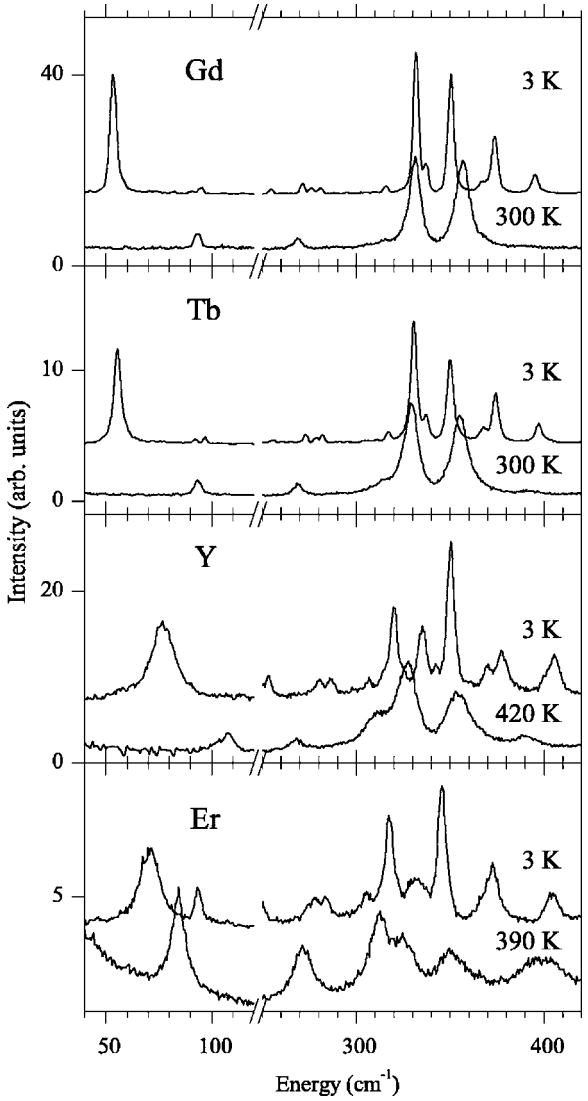

FIG. 5. Comparison of several low-temperature new modes in different $RFe_3(BO_3)_4$. Spectra in ($xx+xy$)-polarization for R=Gd and Tb and partially polarized spectra for R=Y and Er.

of the $B1O_3$ and $B2O_3$ groups, two correspond to the $B2O_3$ ν_3 and ν_4 vibrations, and two to the rotational and translational modes of the $B2O_3$ group. The remaining A_1 mode results from displacements of the iron atom. Table II indicates the origin of crystal modes in the frequency ranges of internal vibrations of the BO_3 molecules.

B. Low-temperature structure $P3_121(D_3^4)$

The primitive cell of the low-temperature structure contains three formula units[8] (60 atoms), which gives 177 vibrational modes. Unique positions for the R and B1 atoms remain, but their symmetry lowers from D_3 in the $R32$ structure to C_2 in the $P3_121$ one. On the contrary, instead of single threefold C_2 symmetry positions for Fe, B2, O1, and O2, there are now two different positions, namely, a threefold C_2 and a sixfold C_1 positions for each of them. O3 oxygen atoms occupy now three different general (C_1) positions.[8] The factor-group analysis of the low-temperature

TABLE I. Observed vibrational modes in several rare-earth iron borates. (a) External modes of the high temperature phase. (b) Internal modes in the high temperature phase. (c) Newly activated modes in the low temperature phase.

(a) External modes ($3A_1 \oplus 11E$)

$NdFe_3(BO_3)_4$			$GdFe_3(BO_3)_4$			$TbFe_3(BO_3)_4$		$ErFe_3(BO_3)_4$		$YFe_3(BO_3)_4$	
A_1	E_{TO}	E_{LO}	A_1	E_{TO}	E_{LO}	A_1	E	A_1	E	A_1	E
180	89	93	180	84	93	180	93	181	84	180	107
298		159	307	160	160	309	159	312	160	312	158
473		193	475	195	198	476	198	472	199	468	200
		232			232		230		225		
	260	266		270	270		270		272		268
	272	281		273	287		287				
	312	332		315	330		330		325		327
	354	356		352	357		355		350		354
		384		391	391		392		395		390
		439		443	443		444		442		441
	475	488			488		480		475		470

(b) Internal modes ($4A_1 \oplus 8E$)

$NdFe_3(BO_3)_4$		$GdFe_3(BO_3)_4$			$TbFe_3(BO_3)_4$		$ErFe_3(BO_3)_4$		$YFe_3(BO_3)_4$	
A_1	E	A_1	E_{TO}	E_{LO}	A_1	E	A_1	E	A_1	E
636	579	638		580	635	579	632	579	631	576
950	625	957	631	633	957	632	960	632		
990	669	990	670	676	988	676	988	675	984	672
1220	734	1230		735	1220	734	1230	730		732
	968			968		966		960		959
	1195									1219
	1218			1212		1214		1220		1230
	1244			1229		1230		1233		1408
	1260		1198	1250		1254				
	1413		1280	1414		1411		1342		

(c) Modes appearing at low temperature phase: $20A_1$ (12 ext. and 8 int.) $\oplus$ $40E$ (24 ext. and 16 int.)

$NdFe_3(BO_3)_4$	$GdFe_3(BO_3)_4$		$TbFe_3(BO_3)_4$		$ErFe_3(BO_3)_4$		$YFe_3(BO_3)_4$	
-	A_1	E	A_1	E	A_1	E	A_1	E
-	53	101	54		72		76	
-	144	114			149		150	111
-	203	167		169	202	170	206	173
-	233	206	232	207	234	208		211
-	244	254	247	256		250	246	253
-	263	276	265	278		278		280
-		281		282		284		287
-		305		306		305		307
-	368	310	368	311				
-	385	337		337				335
-		374		375		373		370
-								378

TABLE I. (*Continued.*)

-		395		398	
-	677	472	679	473	470
-	724	596	723	597	
-		654	953	654	
-		669		670	
-		955		954	
-		968		966	

structure $P3_121$ gives the following optical vibrational modes:

$$\Gamma_{vib}(P3_121) = 27A_1 \oplus 32A_2 \oplus 59E. \quad (5)$$

Carrying out the same procedure as in Sec. IV A, one finds what modes correspond to the external (translational and librational) motions of the R and Fe atoms and of the BO_3 entities and to the internal vibrations of the BO_3 "molecules." The results are summarized in Table III.

V. DISCUSSION

A. Phonons of $RFe_3(BO_3)_4$ in the $R32$ and $P3_121$ phases

First of all, we consider the polarized room-temperature Raman spectra of $RFe_3(BO_3)_4$, R=Nd, Gd, and Tb (Fig. 3). Table I (a), (b) summarizes the observed Raman modes of these iron borates at RT. It has been constructed taking into account the results of the group-theoretical analysis for the $R32$ structure and the frequency ranges for normal modes of the regular planar free ion $(BO_3)^{3-}$ (they are indicated in Fig. 2; see also Tables II and III). The spectra of $ErFe_3(BO_3)_4$ and $YFe_3(BO_3)_4$ were only partially polarized. Comparing the 390 K spectra of $ErFe_3(BO_3)_4$ and the 420 K spectra of $YFe_3(BO_3)_4$ to the RT spectra of other iron borates, we complete Table I for these compounds as well [at room temperature, $ErFe_3(BO_3)_4$ and $YFe_3(BO_3)_4$ are already in the low-temperature phase].

The low-frequency part of the Raman spectrum is dominated by external modes arising from translational motions of the R and Fe atoms and from librational and translational modes of BO_3 groups. The number and polarization properties of the modes observed below 500 cm^{-1} agree with the group-theoretical predictions. All the modes observed in the frequency ranges of the ν_4, ν_2, and ν_1 vibrations of BO_3 correspond well to those derived using the correlation analysis and summarized in Fig. 9. In contrast, there is one extra mode in the region of the ν_3 vibration. Possibly, the strong doublet at about 1220 cm^{-1} in the $(zx+zy)$ polarization arises due to the Fermi resonance[20] between the ν_3 vibrations and an overtone of the ν_4 vibration.

The highest vibrational frequency (originating from the ν_3 vibration of the BO_3 group) observed in $ErFe_3(BO_3)_4$ differs

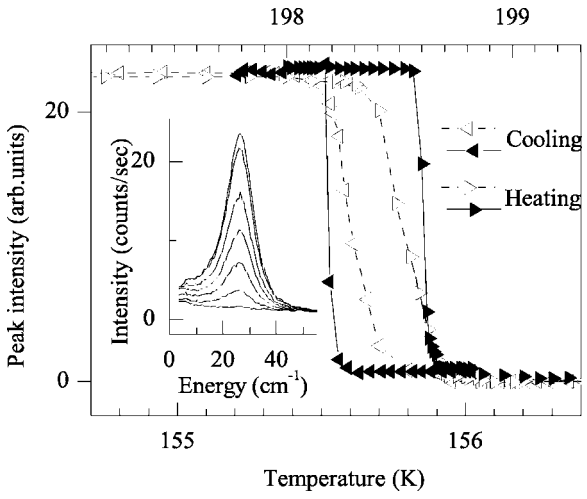

FIG. 6. The lowest-frequency A_1-mode appearing in low-temperature $P3_121$ structure demonstrates hysteresis in a plot of its intensity vs temperature. The data for Gd(Tb)-compound are presented by open (black) triangles. Inset shows this mode during cooling down for temperatures 154.91, 155.03, 155.08, 155.11, 155.16, 155.20, and 155.45 K in Gd compound. The lower-temperature axis refer to R=Gd, the upper one, to Tb.

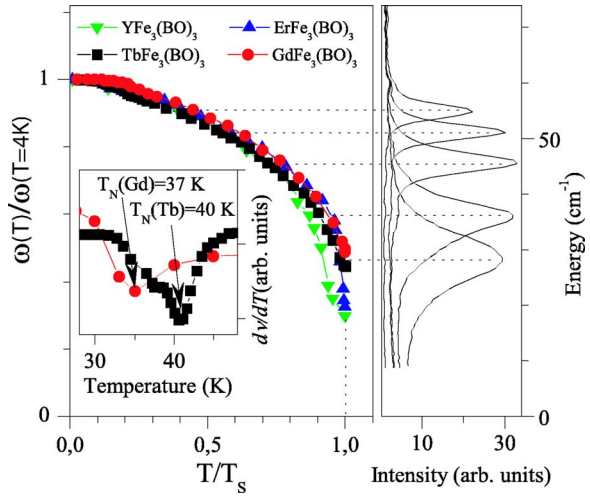

FIG. 7. (Color online) The lowest-frequency mode appears at the phase transition at a finite frequency (characteristic of a first-order transition), but exhibits a high-frequency shift with further lowering the temperature (characteristic of a second-order transition). The inset shows the derivative of the peak frequency in the vicinity of the magnetic ordering temperature, evidencing the coupling of vibrational and magnetic degrees of freedom (see text for discussion).

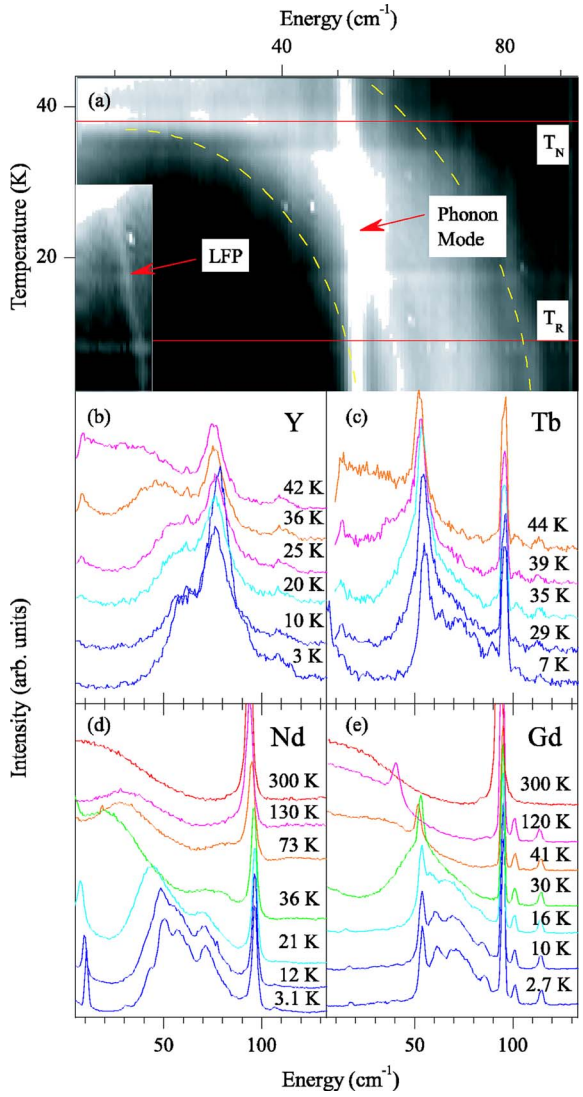

FIG. 8. (Color online) Raman spectra of different $RFe_3(BO_3)_4$ collected in $(xz+yz)$ polarization. Panel (a) shows the opening of a gap in the magnon Raman scattering at $T_N=37$ K for $GdFe_3(BO_3)_4$ (the intensity scale of the left bottom corner of the picture is optimized to evidence the low-frequency mode, and the dotted lines are guides for evidencing the scattering features). The central picture (b,c) shows the magnetic scattering around T_N for $YFe_3(BO_3)_4$ and $TbFe_3(BO_3)_4$. The lower one (d,e) shows the two-magnon spectra in the full temperature range ($2.7\ \text{K} < T < 300\ \text{K}$) for $NdFe_3(BO_3)_4$ on the left and for $GdFe_3(BO_3)_4$ on the right. For the Gd sample a phonon line is evident in proximity of the magnon feature. LFP indicates the low-frequency peak, see the text for the discussion. Above T_N the paramagnon scattering survives up to at least nearly ten times the ordering temperature. Different temperature measurements in panels b–e are depicted with an arbitrary offset for clarity.

markedly from the highest frequencies of both TO($\vec{k} \| c$) and LO($\vec{k} \perp c$) phonons [1280 and 1414 cm^{-1}, respectively, in $GdFe_3(BO_3)_4$]. This is because in our particular nonoriented $ErFe_3(BO_3)_4$ sample, the direction of $\vec{k}$ was arbitrary, while the frequencies of polar E modes depend on the direction of $\vec{k}$.

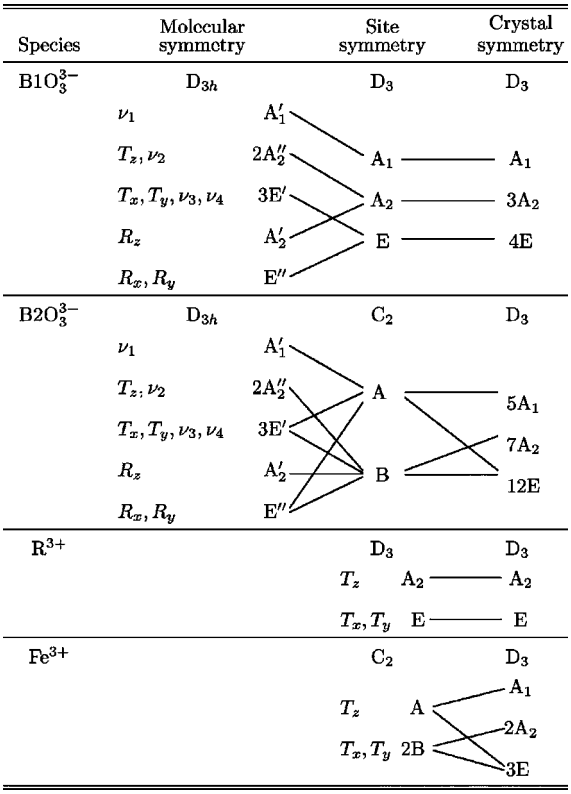

FIG. 9. Correlation scheme for vibrational modes of $RFe_3(BO_3)_4$, space group $R32$.

Summarizing the RT results, it is concluded that (i) the number and symmetries of the Raman modes observed for the $RFe_3(BO_3)_4$ in the high-temperature phase are fully consistent with the predictions of group-theoretical analysis based on the $R32$ space group; (ii) the modes above $\sim 550\ \text{cm}^{-1}$ originate from the internal vibrations of the BO_3 groups, while those below $\sim 550\ \text{cm}^{-1}$ can be considered as external modes.

In the low-temperature $P3_121$ phase, 20 A_1 (12 external and 8 internal) and 40 E (24 external and 16 internal) new modes should appear, according to the results of the group-theoretical analysis (see Table III). These new modes arise for two reasons. First, the symmetries of the local positions for some of the atoms reduce. The intensity of these new modes should depend on the deviation from the former symmetric position. Second, the primitive cell now contains not one but three formula units, leading to an additional Davydov (factor-group) splitting proportional to the strength of interaction between equivalent atoms inside the new primitive cell. Both these effects are, as a rule, small. That is why the number of the observed new modes [$10A_1 \oplus 18E$ in $GdFe_3(BO_3)_4$] is lower than the number predicted by group-theoretical analysis. The same new modes appear below T_s in all the compounds $RFe_3(BO_3)_4$, with R=Gd, Tb, Er, and Y (see Fig. 5 and part (c) of Table I), which strongly suggests the same $P3_121$ low-temperature structure in all of them.

B. Weak first-order structural phase transition

The most characteristic Raman feature that announces the phase transition from the high-temperature $R32$ structure to

TABLE II. Frequency range and assignment of the vibrations of the BO_3 group. The second column lists the assignments for the free ions. The third column shows the expected internal modes and their symmetries in the high-temperature phase of the rare-earth iron borates (the superscripts 1 and 2 refer to the different borate groups in the rare-earth iron borates).

Frequency range (cm^{-1})	BO_3 vibrations (D_{3h})	Crystal vibrations
600	$\nu_4(E')$: in-plane bending	$\nu_4^{(2)}(A_1)+\nu_4^{(1)}(E)+2\nu_4^{(2)}(E)$
700–800	$\nu_2(A_2'')$	$\nu_2^{(2)}(E)$
950	$\nu_1(A_1')$: symmetric breathing	$\nu_1^{(1)}(A_1)+\nu_1^{(2)}(A_1)+\nu_1^{(2)}(E)$
1250–1400	$\nu_3(E')$: asymmetric breathing	$\nu_3^{(2)}(A_1)+\nu_3^{(1)}(E)+\nu_3^{(2)}(E)$

the low-temperature $P3_121$ one is the sudden appearance of a strong new low-frequency mode (see Figs. 4, 6, and 7) in the Raman spectra. As the intensities of new modes are proportional to the squares of atomic displacements, $I \sim \delta^2$, the strongest new mode is believed to be associated with the biggest displacements. A detailed analysis, according to Ref. 8, of the structural changes shows that the biggest displacements are those associated with the BO_3 molecules. In particular, BO_3 triangles, perpendicular to the C_3 axis in the $R32$ structure, tilt by $\sim 7°$ in the $P3_121$ phase; the B1 atoms shift by ~ 0.03 Å from the centers of regular triangles. The shifts of boron ions relative to neighboring oxygen ions create local dipole moments; their triangular arrangement corresponds to an antiferroelectric ordering below the temperature of the structural phase transition. This ordering manifests itself via a strong dielectric anomaly at T_S observed in our preliminary dielectric measurements (Fig. 10).

The structural changes considered above give rise to many new Raman active vibrational modes connected with the BO_3 groups (see Table III), in particular, to $4A_1$ additional librational modes. The energy value of the intense excitation measured is in the typical range of the molecular librations. At 3 K, it is 56, 57, 72, and 76 cm^{-1} for Gd(157), Tb(159), Er(167), and Y(89) compounds, respectively. As the values for the Er and Y compounds are very close, notwithstanding a big difference in atomic masses of Er and Y, we conclude that the rare earth does not take part in this lowest-frequency vibration. A difference between the values for the compounds with relatively big (Gd, Tb) and small (Er, Y) ions comes from the difference in interatomic distances and, hence, force constants. The ensemble of these observations strongly suggests that the phase transition in $RFe_3(BO_3)_4$ is correlated to a rotational mode of the BO_3 groups.

The abrupt appearance of new phonon modes and the hysteresis observed for their intensities when approaching T_S from different sides indicate the first-order character of the phase transition. The energy of the low-frequency mode strongly increases upon lowering the temperature below T_S (Fig. 7). At the lower temperature (3 K), the frequency of the mode has more than doubled. Such an anomalously large shift is typical for soft modes that announce a second-order structural phase transition. Apparently, we deal with a so-called weak first-order phase transition. It is worth noting that the lowering of the symmetry from $R32$ (D_3^7) to $P3_121$ (D_3^4) is, indeed, also compatible with a second-order phase transition.[21] Thus, the observed first-order character of the phase transition does not depend on symmetry changes but rather can arise from the third-order therm in the Landau expansion of the crystal free energy h, allowed by the crystal symmetry, or from the negative sign of the fourth-order coefficient u

$$G = G_0 + rQ^2 + hQ^3 + uQ^4 + \cdots, \tag{6}$$

where Q is the order parameter.[22]

Figure 11 shows the temperatures of the structural phase transition in $RFe_3(BO_3)_4$ plotted vs ionic radii of R^{3+}, as determined in Ref. 9 for powder samples and in the present study for single crystals. A mismatch between our data and those of Ref. 9 could arise from a rather poor quality of the

TABLE III. The origin of vibrations for two structural modifications of $RFe_3(BO_3)_4$ and the new modes that should appear below the temperature of the structural phase transition T_s.

species	$T>T_s$: $R32$ (D_3^7)	$T<T_s$: $P3_121$ (D_3^4)	New modes
R	$A_2 \oplus E$	$A_1 \oplus 2A_2 \oplus 3E$	$A_1 \oplus 2E \oplus A_2$
Fe	$A_1 \oplus 2A_2 \oplus 3E$	$4A_1 \oplus 5A_2 \oplus 9E$	$3A_1 \oplus 6E \oplus 3A_2$
External BO_3			
Translational	$A_1 \oplus 3A_2 \oplus 4E$	$5A_1 \oplus 7A_2 \oplus 12E$	$4A_1 \oplus 8E \oplus 4A_2$
Librational	$A_1 \oplus 3A_2 \oplus 4E$	$5A_1 \oplus 7A_2 \oplus 12E$	$4A_1 \oplus 8E \oplus 4A_2$
Internal BO_3	$4A_1 \oplus 4A_2 \oplus 8E$	$12A_1 \oplus 12A_2 \oplus 24E$	$8A_1 \oplus 16E \oplus 8A_2$
Total	$7A_1 \oplus 13A_2 \oplus 20E$	$27A_1 \oplus 33A_2 \oplus 60E$	$20A_1 \oplus 40E \oplus 20A_2$

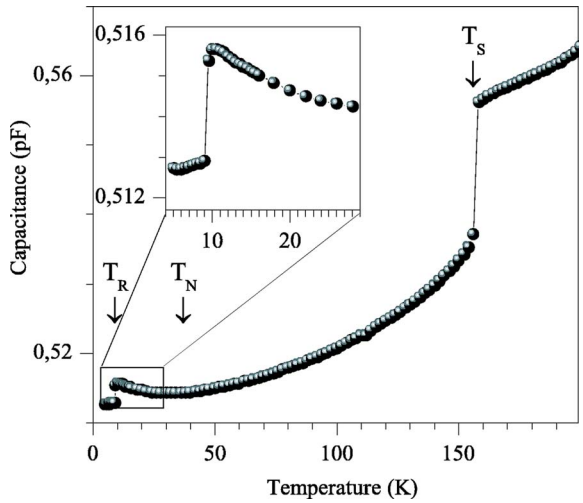

FIG. 10. (Color online) Dielectric measurements of $GdFe_3(BO_3)_4$. The structural phase transition is made evident by a step in the capacitance at T_S. No evidence is found of the Fe ordering phase transition at T_N, while the capacitance shows a discontinuity at the spin-reorientation phase transition at T_R (displayed in more detail in the inset).

Er and Y iron borate single crystals. A further study is necessary to clarify this question.

Finally, we note that $NdFe_3(BO_3)_4$ preserves the $R32$ structure down to the lowest temperatures, while $RFe_3(BO_3)_4$ with R^{3+} smaller than Tb^{3+} have the low-temperature $P3_121$ structure already at room temperature.

C. Magnetoelastic coupling

The inset of Fig. 7 shows the derivative of the peak frequency of the strongest new A_1 mode as a function of temperature in the vicinity of the magnetic ordering temperature T_N. The coupling of vibrational and magnetic degrees of freedom is evident. The discontinuity in the phonon frequency observed at $T=T_N$ is ascribed to magnetoelastic coupling. The magnetic ordering causes spontaneous magnetostriction, that is, atomic displacements. The latter, evidently, influence vibrational frequencies. Recently, Ref. 4 reported on the study of magnetoelectric and magnetoelastic properties of $GdFe_3(BO_3)_4$. A strict correlation between both has been shown experimentally and discussed theoretically. The authors of Ref. 4 assumed that, below T_N, the crystal symmetry lowers, due to magnetoelastic coupling with spontaneous magnetic moments lying in the *ab* plane. This breaks the symmetry of the antiferroelectric arrangement of the electric dipole moments in the $P3_121$ structure and leads to the appearance of an electric polarization, which could be responsible for the weak growth of the dielectric constant in the temperature region $T_R<T<T_N$ (see also Fig. 10).[4] The proposed lowering of crystal symmetry below T_N, however, should result in the appearance of new vibrational modes. No indications for additional modes below T_N have been found. This does not necessarily mean that the model by Zvezdin *et al.*[4] is in error. It might very well be that the structural changes are simply too small to be detected by Raman scattering.

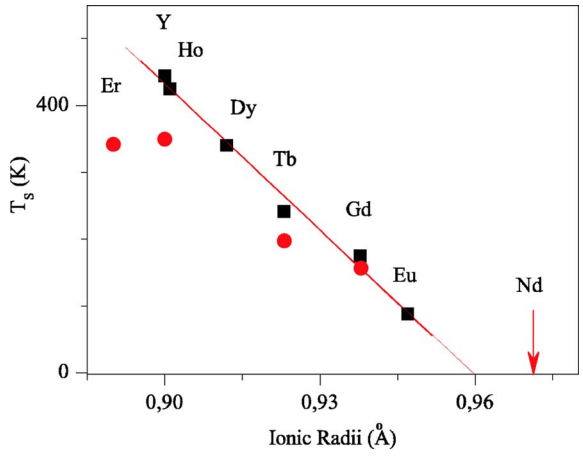

FIG. 11. (Color online) Temperatures of the structural phase transitions for different $RFe_3(BO_3)_4$ as a function of the ionic radius. Our data on single crystals are shown by circles, those of Ref. 9 on powder samples are presented by squares.

As Ref. 4 suggests, the spin-reorientation first-order phase transition at T_R into the antiferromagnetic configuration of spins parallel to the *c* axis recovers the $P3_121$ structure (that does not allow the presence of the electric dipole moment) and, therefore, is expected to be accompanied by a jump of the dielectric constant. As is clear from Fig. 10, the dielectric function indeed exhibits such a jump, thereby strongly supporting the suggested scenario.

D. Magnetic scattering

As discussed in the introduction, due to the structural properties of the $RFe_3(BO_3)_4$ family, Fe atoms (S=5/2) are arranged in helicoidal chains. As a result, the Fe-Fe distance inside the chain is substantially smaller than the distance between different chains. The main exchange interaction is therefore expected to be between Fe ions on the same chain ($J_{\|}\rangle\rangle J_{\perp}$), suggesting that low dimensionality could play a crucial role in the magnetic properties of the family. This, together with the presence of two coupled magnetic sublattices makes the compounds with magnetic R^{3+} ions good candidates for exotic magnetic ground states.

A complex magnetic behavior has indeed been found and widely discussed in $GdFe_3(BO_3)_4$. The first magnetization measurements on oriented single crystals were interpreted under the assumption that both Fe and Gd subsystems order antiferromagnetically at $T_N=40$ K.[11] In this model, below 10 K, the total magnetic moment of the three Fe sublattices (S=5/2) oriented at polar angles ~60° to the *c* axis is compensated by the Gd moment (S=7/2) oriented along the *c* axis. Sharp singularities in magnetization in the magnetic field $H||c$ observed below 10 K were attributed to spin-flop transitions in the Fe subsystem. It was assumed further that in the range of temperatures between 10 and 40 K the magnetic moments of every Fe sublattice fall into the *ab* plane, perpendicular to the *c* axis, preserving the 120° azimuthal orientation.

This model was later reconsidered in Ref. 12. It has been suggested, on the basis of the analysis of the Nd-probe spec-

tra and of the specific heat data, that the Gd subsystem does not undergo a magnetic phase transition at T_N but only gets polarized by the Fe subsystem. The following model has been put forward. At T_N=37 K, the iron magnetic moments order antiferromagnetically in the direction perpendicular to the c axis and polarize the Gd subsystem. Below T_R=9 K, the magnetic moments order antiferromagnetically along the c axis. The temperature T_R=9 K corresponds to a first-order spin-reorientation magnetic phase transition.[12] Simultaneously and independently, the same conclusion has been drawn in Ref. 13, where magnetic structures and magnetic phase transitions in $GdFe_3(BO_3)_4$ were studied using antiferromagnetic resonance experiments. This study revealed also a detailed picture of the magnetic structure and anisotropy for different magnetic phases in $GdFe_3(BO_3)_4$ as a function of both temperature and magnetic field. At T_N=38 K, the Fe magnetic subsystem orders into a two-sublattice collinear easy-plane antiferromagnet and polarizes the Gd spins, which also form a two-sublattice antiferromagnetic subsystem. The anisotropy constant of the Gd subsystem has an opposite sign to that of the Fe subsystem. The Gd contribution to the total anisotropy energy grows with lowering the temperature, in conjunction with the growing polarization of the Gd subsystem, and becomes appreciable below~20 K. At T_R=10 K, the total energy of anisotropy changes its sign, which results in the spontaneous spin reorientation transition.

The long-range order of the spins on the iron subsystem manifests itself in the inelastic light scattering experiments with two main features. The first one, as reported in Fig. 8, is the arising of a low-frequency peak (LFP) at ~10 cm^{-1} in $NdFe_3(BO_3)_4$ and at ~18 cm^{-1} in $GdFe_3(BO_3)_4$. These peaks soften and broaden upon approaching T_N. The energy of 10 cm^{-1} in $NdFe_3(BO_3)_4$ has been identified, by absorption spectroscopy of Nd^{3+} crystal-field levels, as the exchange splitting energy of the Nd^{3+} ground Kramers doublet at 5 K arising from the interaction with the ordered Fe sublattice.[10] The temperature dependences of the frequency and the linewidth of the Raman LFP are the same as those of the ground-state splitting and, respectively, the ground-level width found from optical spectroscopy.[10] Therefore, the 10 cm^{-1} Raman mode observed in $NdFe_3(BO_3)_4$ is assigned to spin flip scattering on a single Nd^{3+} moment in the effective field created by the Fe sublattice. Most likely, the 18 cm^{-1} excitation observed in $GdFe_3(BO_3)_4$ has the same origin. The absence of LFP in Raman scattering of $YFe_3(BO_3)_4$ with nonmagnetic Y^{3+} (see Fig. 8) is in favor of such interpretation. The crystal field of $RFe_3(BO_3)_4$ splits the ground-state multiplet of an ion R^{3+} with odd number of electrons into Γ_4 and Γ_{56} Kramers doublets within the D_3 site symmetry. The analysis of Raman selection rules for the ground-state spin flip scattering shows that in the case of the Γ_4 ground state all the components of the Raman tensor are allowed while, in the case of the Γ_{56} ground state, only the antisymmetric xy-yx component is Raman active. Thus, a relatively strong (xz) Raman LFP of $NdFe_3(BO_3)_4$ points to the Γ_4 symmetry of the Nd^{3+} ground state.

The second major feature of the iron spin ordering is the arising of a broad structured scattering band around 60 cm^{-1} ascribed to two-magnon Raman scattering involving the creation of a pair of magnons with wave vectors $\vec{k}$ and $-\vec{k}$. Below the Néel temperature, this is a characteristic feature for all the different compound investigated of the $RFe_3(BO_3)_4$ family (R=Y, Er, Tb, Gd and Nd). Figure 8 shows the temperature evolution of this broad signature of magnetic scattering. The spectra reported in Fig. 8 are observed in the $(xz+yz)$ polarization only. No evidence of magnetic scattering is found when the $\vec{k}$ vector of light is parallel to the c axis $[z(xx+yy+xy)z]$.

As discussed in Sec. IV C, $NdFe_3(BO_3)_4$ does not undergo a structural phase transition and the crystal space group remains the high-temperature one ($R32$), while the symmetry of all the other compounds investigated (for R=Gd, Tb, Y, and Er) is reduced to the space group $P3_121$. It is evident from Fig. 8 that the magnetic scattering spectra of all iron borates are quite similar. Thus, the presence of inequivalent Fe chains[8] in the low-temperature structure of $RFe_3(BO_3)_4$, R=Gd, Tb, Y, and Er does not strongly affect the magnetic excitation spectra, and the spectra can be analyzed taking into account only the four different magnetic ions present in the $R32$ unit cell (three Fe^{3+} ions and one R^{3+} ion). Still, a rather complicated two-magnon spectrum is expected, strongly depending on the anisotropy parameters. At the lowest temperature reached (T=2.7 K), the two-magnon spectra indeed show a complex structure exhibiting at least three main peaks (Fig. 8). As the most efficient mechanism of two-magnon scattering in antiferromagnets is usually the exchange-scattering mechanism and the strongest exchange interaction is between the iron atoms along the helicoidal chains, these peaks presumably arise from three magnon branches representing spin excitations on the iron chains.

The broad magnetic scattering feature of Gd, Tb, Er, and Y compounds is approximately centered around $\simeq$70 cm^{-1}, while the one of Nd is centered at lower frequency ($\simeq$60 cm^{-1}). This suggests that the bigger ionic radius of Nd^{3+} causes the interatomic Fe-Fe distances to be larger and, therefore, the exchange interaction to be smaller; this would be consistent with the scaling of T_N with the rare earth's ionic radii.[9] Unfortunately, because of the presence of phonon modes at the same frequency of the magnetic excitation, it is not possible to determine the frequency scaling of the magnetic scattering among the other compounds (Gd, Tb, Er, and Y) to confirm this.

At the temperature of the spin-reorientational transition (T_R), no drastic changes are observed in the magnon spectra. This observation confirms that the observed scattering is mainly due to magnetic excitations on the Fe^{3+} chains and sheds light on the proposed exotic magnetic ordering of Fe spins for the $GdFe_3(BO_3)_4$ compound. The configuration with 120° angle between nearest-neighbor Fe^{3+} spins for $T_N > T > T_R$, which then reorient at T_R into an easy axis antiferromagnet along the c axis as proposed in Ref. 11 is not consistent with our observation. Such a drastic change in the spin configuration would induce a major change in the two-magnon dispersion and inelastic scattering spectra. The picture of a reorientational phase transition at T_R, as proposed in Refs. 12 and 13, survives assuming an easy-axis and/or easy-plane anisotropy perpendicular to the c axis in the temperature region $T_R < T < T_N$. Indeed, considering a simple

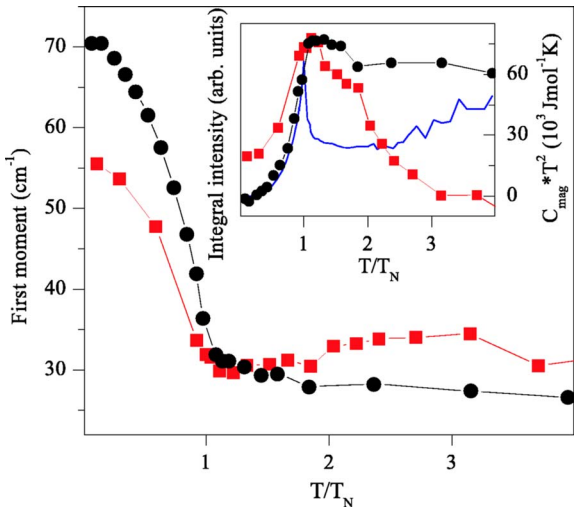

FIG. 12. (Color online) First moment $\langle\omega\rangle$ of the magnetic excitation vs temperature calculated from 5 to 85 cm^{-1} for $GdFe_3(BO_3)_4$ (circles) and $NdFe_3(BO_3)_4$ (squares). The inset shows the integrated intensity of the magnetic signal at different temperature, compared to the magnetic heat capacity of $YFe_3(BO_3)_4$ (solid line) (Ref. 9).

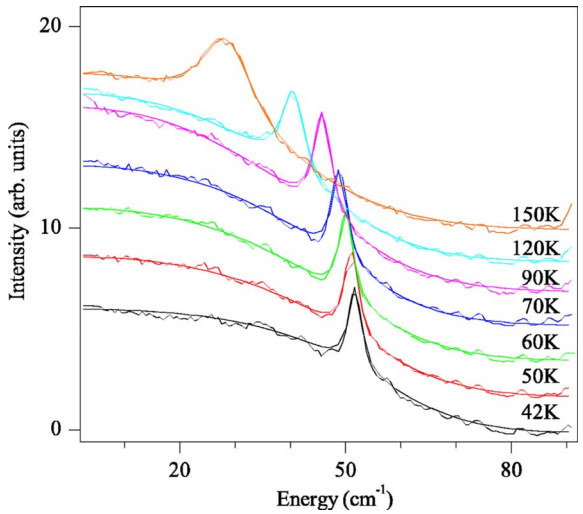

FIG. 13. (Color online) Low-frequency Raman scattering above the Néel temperature for $GdFe_3(BO_3)_4$. The different temperature are depicted with an offset for clarity. The paramagnon scattering is present up to almost $4T_N$. The fit is obtained with an fenomenological curve $f(\omega)=\frac{G}{1+aG}+L$, where G is a Gaussian distribution centered at zero frequency, and L is a Lorenzian distribution to take into account the presence of the vibrational mode (see text for discussion).

Heisenberg-type Hamiltonian, where the interaction depends only on the nearest-neighbor scalar product, an easy axis anisotropy perpendicular or parallel to the c axis would produce similar magnetic excitation spectra and, therefore, similar two-magnon spectra.

A striking feature of the magnetic scattering, as shown in Fig. 8, is the persistence of the magnetic scattering in an anomalous shape up to extremely high temperature above T_N. In the three-dimensional antiferromagnet NiF_2, this "paramagnon scattering" has been observed well into the paramagnetic phase up to $4T_N$.[23] The first moment of the frequency $\langle\omega\rangle$ as a function of temperature in NiF_2 and MnF_2 exhibited a fast decrease to lower frequency ($\simeq$10% of the "zero-temperature value") at T_N and a subsequent smooth decrease to zero for $T>T_N$, in excellent qualitative agreement with the theory prediction for the moments.[24] Also in the case of $RFe_3(BO_3)_4$ the two-magnon spectrum softens, continuously, its frequency approaching the Néel temperature (Fig. 8). Yet, surprisingly, the paramagnon scattering survives at all measured temperatures above T_N (i.e., up to about ten times T_N). As reported in Fig. 12, the first moment of the excitation decreases at T_N less than expected and approaches zero only very slowly above T_N. Considering $NdFe_3(BO_3)_4$, the minimum at T_N and subsequent increases with temperature up to 2.5 T_N of the first moment is possibly due to the presence of luminescence lines overlapping with features of the magnetic scattering. This is likely also the origin of the temperature shift to high frequency (lower absolute energy) of the excitation observed at around 80 cm^{-1}.

From a theoretical point of view the presence of quasielastic scattering well into the paramagnetic phase of three-dimensional antiferromagnets has been ascribed to two possible origins, namely, spin diffusion[25] and spin density fluctuations or energy diffusion.[26] In the scenario of spin diffusion, absent in a perfect one-dimensional system, the four-spin correlation function (describing the Raman response) is well approximated by a Gaussian shape centered at zero energy. In contrast, for the energy diffusion scenario one expects a Lorentzian line shape in the absence of strong spin-lattice interactions. The integrated intensity I_m in the energy diffusion scenario is expected to follow the magnetic contribution to the heat capacity C_m as $I_m \propto C_m T^2$.[25,26] In the presence of strong spin-lattice coupling, this later relation is expected to remain valid, even though the low-energy scattering is expected to broaden significantly due to the rapid relaxation of the magnetic excitation energy into the lattice.

The shape of the low-energy scattering feature in the paramagnetic phase is different from any previously reported. Neither a Lorenzian nor a Gaussian distribution can fit our data. This anomalous shape of the paramagnon scattering continuum is a common feature of all the compounds investigated; Fig. 13 depicts the observed spectra of $GdFe_3(BO_3)_4$ as an example. The observation that the spectra cannot be modeled with either a Gaussian nor a Lorentzian response might evidence the presence of important spin-lattice interactions, in line with the observations discussed in Sec. IV. A comparison of the integrated intensity for $GdFe_3(BO_3)_4$ and $NdFe_3(BO_3)_4$ to the magnetic heat capacity determined by Hinatsu *et al.*[9] (see inset Fig. 12) for $YFe_3(BO_3)_4$ does not show a fair agreement in the "paramagnetic" phase, even though there is a good correlation below the phase transition. Apparently, energy diffusion, combined with spin-lattice coupling does not explain the observed scattering. On the other hand, as shown in Fig. 13, the spectra for $GdFe_3(BO_3)_4$ can be fitted nicely at all temperature with a broad phenomenological function consisting of a renormalized Gaussian distribution $I(\omega)=\frac{G(\omega)}{1+\alpha G(\omega)}+L$, where $G(\omega)$ is a pure Gaussian, and $L(\omega)$ is a Lorentzian to account for the phonon line observed in the spectra. This equation is reminescent of the

response function of interacting magnons in low-dimensional quantum spin systems, although it would be unclear why this would still hold for a $S=5/2$ system at high temperatures. At present one cannot draw a definite conclusion, but the results do strongly suggest that short-range order correlations in the spin system survive up to quite high temperatures. Most likely an interplay between the low dimensionality and strong spin-lattice interactions are responsible for the observed unique behavior of the magnetic scattering up to several times T_N and deserves further studies.

VI. SUMMARY

In summary, structural, magnetic, and magnetoelastic properties of various members of the $RFe_3(BO_3)_4$ family (R =Gd, Tb, Nd, Er, and Y) have been studied using primarily inelastic light scattering. The compounds show a weak first-order structural phase transition, which results in the activation of a strong mode of BO_3 librational nature, and its subsequent temperature evolution. The scattering spectra observed in the low-temperature phase are fully consistent with the low-temperature structure reported earlier. A detailed analysis of the vibrational spectra at the temperature of the magnetic ordering transition showed a strong magnetoelastic coupling for all the compounds. The analysis of the two-magnon Raman scattering in the magnetic phases showed qualitatively similar scattering spectra for the five compounds investigated, evidencing that the structural differences between them do not strongly affect the magnetism and the magnetic excitation spectra. Finally, an unprecedented an intriguing paramagnon scattering continuum up to quite high temperatures. The origin of this scattering does not seem to be the usual energy diffusion observed in a variety of other magnetic system and seems to indicate the presence of short-range order spin-spin correlations arising from the low-dimensional nature of these compounds.

ACKNOWLEDGMENTS

The authors are grateful to M. Mostovoy and D. Khomskii for valuable discussions. This work was partially supported by the Stichting voor Fundamenteel Onderzoek der Materie [(FOM), financially supported by the Nederlandse Organisatie voor Wetenschappelijk Onderzoek (NWO)]. S.A.K., M.N.P., and L.N.B. acknowledge the support of the Russian Foundation for Basic Research, Grants No. 04-02-17346 and No. 03-02-16286, and the Russian Academy of Sciences under the Programs for Basic Research.

*Electronic address: d.fausti@rug.nl
†Electronic address: P.H.M.van.Loosdrecht@rug.nl

[1] D. Jaque, J. Alloys Compd. **323-324**, 204 (2001).
[2] A. Brenier, C. Tu, Z. Zhu, and B. Wu, Appl. Phys. Lett. **84**, 2034 (2004).
[3] X. Chen, Z. Luo, D. Jaque, J. J. Romero, J. Garcia Solé, Y. Huang, A. Jiang, and C. Tu, J. Phys.: Condens. Matter **13**, 1171 (2001).
[4] A. K. Zvezdin, S. S. Krotov, A. M. Kadomtseva, G. P. Vorob'ev, Y. F. Popov, A. P. Pyatakov, L. N. Bezmaternykh, and E. Popova, JETP Lett. **81**, 272 (2005).
[5] J. C. Joubert, W. B. White, and R. Roy, J. Appl. Crystallogr. **1**, 318 (1968).
[6] E. L. Belokoneva, L. I. Alshinskaya, M. A. Simonov, N. I. Leonyuk, T. I. Timchenko, and N. V. Belov, J. Struct Khimii **20**, 542 (1979).
[7] J. A. Campa, C. Cascales, E. Gutierrez-Puebla, M. A. Monge, I. Rasines, and C. Ruiz-Valero, Chem. Mater. **9**, 237 (1997).
[8] S. A. Klimin, D. Fausti, A. Meetsma, L. N. Bezmaternykh, P. H. M. van Loosdrecht, and T. T. M. Palstra, Acta Crystallogr., Sect. B: Struct. Sci. **61**, 481 (2005).
[9] Y. Hinatsu, Y. Doi, K. Ito, K. Wakeshima, and A. Alemi, J. Solid State Chem. **172**, 438 (2003).
[10] E. P. Chukalina, D. Y. Kuritsin, M. N. Popova, L. N. Bezmaternykh, S. A. Kharlamova, and V. L. Temerov, Phys. Lett. A **322**, 239 (2004).
[11] D. Balaev, L. N. Bezmaternyh, I. A. Gudim, V. L. Temerov, S. G. Ovchinnikov, and S. A. Kharlamova, J. Magn. Magn. Mater. **258-259**, 532 (2003).
[12] R. Z. Levitin, E. A. Popova, R. M. Chtsherbov, A. N. Vasiliev, M. N. Popova, E. P. Chukalina, S. A. Klimin, P. H. M. van Loosdrecht, D. Fausti, and L. N. Bezmaternykh, JETP Lett. **79**, 423 (2004).
[13] A. I. Pancratz, G. A. Petrakovskii, L. N. Bezmaternykh, and O. A. Bayukov, JETP **99**, 766 (2004).
[14] A. G. Gavriliuk, S. A. Kharlamova, I. S. Lyubutin, I. A. Troyan, E. S. Ovchinnikov, A. M. Potsjelujko, M. I. Eremets, and R. Böhler, JETP Lett. **80**, 426 (2004).
[15] A. de Andres, F. Agullo-Rueda, S. Taboada, C. Cascales, J. Campa, C. Ruiz-Valero, and I. Rasines, J. Alloys Compd. **250**, 396 (1997).
[16] L. N. Bezmaternykh, V. L. Temerov, I. A. Gudim, and N. A. Stolbovaya, Crystallogr. Rep. **50**(Suppl. 1), S97 (2005).
[17] L. N. Bezmaternykh, S. A. Kharlamova, and V. L. Temerov, Crystallogr. Rep. **49**, 855 (2004).
[18] D. L. Rousseau, R. P. Bauman, and S. P. S. Porto, J. Raman Spectrosc. **10**, 253 (1981).
[19] B. N. Mavrin, Opt. Spektrosk. **49**, 79 (1980).
[20] G. Herzberg, *Infrared and Raman Spectra of Polyatomic Molecules* (Van Nostrand Reinhold, New York, 1945).
[21] L. D. Landau and E. M. Lifshitz, *Statistical Physics* (Pergamon Press, Oxford, 1980).
[22] A. D. Bruce and R. A. Cowley, *Structural Phase Transitions* (Taylor & Francis, London, 1981).
[23] P. A. Fleury, Phys. Rev. **180**, 591 (1969).
[24] M. G. Cottam and D. J. Lockwood, *Light Scattering in Magnetic Solids* (Willey, New York, 1986).
[25] P. M. Richards and W. J. Brya, Phys. Rev. B **9**, 3044 (1974).
[26] J. W. Halley, Phys. Rev. Lett. **41**, 1605 (1978).